International Journal of Analysis and Applications

Analytical Solution of Rate Equations Including Frequency Chirp of Modulated Quantum-Well Laser with Carrier Transport Processes

Moustafa Ahmed[1,*], Maan Al-Alhumaidi[1], Awy Sayed[2]

[1]*Department of Physics, Faculty of Science, King Abdulaziz University, 80203, Jeddah, Saudi Arabia*
[2]*Information Technology Department, Faculty of Computing and Information Technology, King Abdulaziz University, 80203, Jeddah, Saudi Arabia*
**Corresponding author:* mhafidh@kau.edu.sa

ABSTRACT. When used as light sources in modern fiber communication systems, the modulation bandwidth and chirp are crucial characteristics of high-speed quantum well (QW) lasers. These parameters are primarily constrained by two factors; namely, the transport of charge carriers in the separate confinement heterojunction (SCH) layer and their escape processes in the QW. To analyze the frequency chirp theoretically, a fourth rate equation is added to the existing system of three coupled rate equations, which describe the photon number in the QW and carrier numbers in both the QW and SCH layers. This study employs small-signal analysis to linearize these coupled equations and derives analytical expressions for both the intensity modulation (IM) response and its associated frequency chirp. The chirp is quantified using two metrics, first the chirp per modulated current (CCR), and second the chirp per modulated power (CPR). These analytical expressions are presented in a generalized form, making them applicable to any nonlinear gain mathematical formulation found in the literature. Through numerical calculations applied to high-speed QW lasers, we investigate the individual effects of transport and escape times on the frequency chirp. Our findings demonstrate that CCR reaches its minimum under two specific conditions: when the transport process is relaxed with a relatively long transport time, and when carrier escape in the QW occurs rapidly with a very short escape time. Notably, we found that CPR remains independent of the transport processes.

1. INTRODUCTION

Quantum-well (QW) lasers have become indispensable components in modern fiber communication systems, owing to their superior performance characteristics and potential for

Received Sep. 14, 2024

2020 Mathematics Subject Classification. 78A40.

Key words and phrases. quantum well laser; carrier transport; small-signal analysis.

https://doi.org/10.28924/2291-8639-22-2024-215

ISSN: 2291-8639

high-speed modulation. Among the critical parameters that define the efficacy of these lasers in optical communication networks are the modulation bandwidth and frequency chirp [1], [2] . The performance of QW lasers is primarily constrained by two fundamental processes; namely, the transport of charge carriers within the separate confinement heterojunction (SCH) layer and the escape mechanisms of carriers from the quantum well [3]–[7]. These transport processes are influenced by two main factors: the ambipolar diffusion time and carrier capture in the SCH layers, and the thermionic emission (or carrier escape time) from the well. The transport time across the SCH layer significantly contributes to a low-frequency rolloff in the modulation response [8]–[10], substantially limiting the modulation bandwidth. In QW lasers, which typically have relatively small optical confinement factors, variations in carrier density and subsequent changes in refractive index introduce an additional chirp component [11]-[15]. Research by Ribeiro et al. [16] demonstrated that carrier transport effects can substantially alter both the frequency modulation pattern and frequency chirp characteristics. This chirp must be minimized for efficient laser applications, particularly in fiber links, to reduce the fiber dispersion effect on the transmitted signal [17]. The chirp per modulated power ratio (CPR) serves as an effective metric for evaluating the frequency chirp that accompanies intensity modulation [18]. Consequently, controlling and reducing frequency chirp in QW lasers necessitates a thorough understanding of how chirp depends on transport processes within the QW structure. While previous literature has addressed the impacts of SCH layer transport processes and QW carrier capture on frequency chirp in general [11]-[14], and on CPR [19], in particular, the individual contributions of these processes to chirp behavior have not been thoroughly investigated. This gap in understanding warrants further research to optimize QW laser performance in optical communication systems.

The analysis of intensity modulation properties in QW lasers typically employs a three-coupled rate-equations model. This model describes the temporal evolution of photon density emitted in the QW and carrier densities in both the QW and barrier regions, while accounting for carrier transport effects [10]. These rate equations can be solved through various numerical integration techniques. In recent work, the authors developed a small-signal modeling approach to analyze the intensity modulation (IM) response in QW lasers [20]. This approach linearizes the rate equations and enables investigation of how the escape and capture lifetimes between the SCH layer and QW affect laser performance. To analyze frequency chirp in QW lasers, an additional fourth equation is required to describe the rate of change in the optical phase of the oscillating mode. While necessary for comprehensive analysis, this additional equation increases both the complexity of the model and the coupling between rate equations.

In this study, we expand upon the model presented in [20] to incorporate the phase (frequency) variations associated with intensity modulation and develop analytical formulas for both the IM response and frequency chirp. The chirp is evaluated using both CCR and CPR. We apply these formulas to analyze a high-speed QW laser, investigating how transport processes in the SCH and QW layers affect the modulation bandwidth and frequency chirp. The transport processes in the SCH layer encompass both carrier capture by the QW and diffusion across the SCH. The total transport time in the SCH layer comprises both the capture time and diffusion periods for holes and electrons. We adjust the range of escape time in the QW according to its relationship with the SCH layer thickness. Gain suppression plays a crucial role in characterizing the relationship between intensity and frequency modulation behavior of laser diodes and is the primary effect causing damping in intensity modulation [21], [22]. Therefore, we derive expressions for the IM response and chirp that accommodate any form of nonlinear gain documented in the literature. These derived expressions enable a comparison of how different gain formulations influence the modulation characteristics of QW lasers. This approach ensures the broad applicability of our findings across different laser configurations and operating conditions Through detailed numerical calculations applied to high-speed QW lasers, we investigate the individual effects of transport and escape times on the frequency chirp. Our findings reveal that the chirp CCR reaches its minimum when two conditions are met: first, when the transport process is relaxed with a relatively long transport time, and second, when carrier escape in the QW occurs rapidly, resulting in a very short escape time. Conversely, the chirp CPR demonstrates independence from the transport processes.

The findings of this research have significant implications for the design and optimization of QW lasers, potentially leading to improved performance in next-generation optical communication networks. By elucidating the intricate relationships between carrier transport processes, escape mechanisms and laser chirp, this study contributes to the ongoing efforts to push the boundaries of high-speed optical communications.

2. RATE EQUATION MODEL OF QW LASER

In the SCH-QW laser, charge neutrality is assumed to hold in the entire intrinsic SCH region and holes dominate the carrier dynamics. The exterior edges of the left and right SCH regions are used to inject the electrons and holes, respectively, into the QW. Before recombination by stimulated emission, the injected carriers diffuse into the SCH region and are captured in the QWs [23]. In addition, thermionic emission works against carrier capture and reduces the QW structure's total carrier capture efficiency [24]. That is, two terms that stand in for carrier transport

across the SCH (represented by transport time τ_{tr}) and escape (represented by escape time τ_{esc}) into or from the well, respectively, are used to model how the carrier density in the barrier states above the QW's and the carrier density in the QW couple to one another. The associated rate equations that describe the temporal changes in the carrier number $N(t)$ and photon number $S(t)$ in the QW, optical phase $\theta(t)$, and carrier number $N_B(t)$ in the SCH or barrier layer [25] are:

$$\frac{dS}{dt} = \Gamma G(N,S)S - \frac{S}{\tau_p} + \beta_{sp}\frac{N}{\tau_e} \tag{2.1}$$

$$\frac{dN_B}{dt} = \frac{I}{e} - \frac{N_B}{\tau_{tr}} + \frac{N}{\tau_{esc}} \tag{2.2}$$

$$\frac{dN}{dt} = \frac{N_B}{\tau_{tr}} - \frac{N}{\tau_{esc}} - \frac{N}{\tau_e} - G(N,S)S \tag{2.3}$$

$$\frac{d\theta}{dt} = \frac{1}{2\pi}\Delta\nu(t) = \frac{1}{2\pi}\left[\nu - \nu_0 + \frac{\alpha}{2}\left(\Gamma G(N,S) - \frac{1}{\tau_p}\right)\right] \tag{2.4}$$

The function $G(N,S)$ defines the optical gain. Since there are different forms of optical gain in literature, especially when including the nonlinear gain suppression, we are interested in this paper to introduce both the intensity modulation response and the associated frequency chirp in terms of the function $G(N,S)$ in general. Therefore the results could be applied to any of the reported nonlinear gain forms, such as

$$G(N.S) = \begin{cases} \frac{g_0}{V}\left(N - N_g\right) - BS & (a) \\ \frac{\frac{g_0}{V}(N-N_g)}{1+\varepsilon S} & (b) \\ \frac{\frac{g_0}{V}(N-N_g)}{\sqrt{1+\varepsilon S}} & (c) \\ \frac{g_0}{V}\left(N - N_g\right)(1-\varepsilon S) & (d) \end{cases} \tag{2.5}$$

The term $\frac{g_0}{V}\left(N - N_g\right)$ represents the linear gain, where g_0 is the slope gain coefficient, and N_g is the carrier density at transparency. The gain form (5-a) was derived by Yamada and Suematsu [26] and Ahmed and Yamada [27] based on a third-order perturbation approach, with B representing the coefficient of gain suppression. The form (5-b) was originally suggested by Channin et al. [28] and is valid for $S \geq 0$ to describe damping in the IM response of the diode laser, while the form (5-c) was suggested by Agrawal et al. [29]. These two forms were derived for the cases of homogeneous and inhomogeneous gain broadening by Ahmed and Yamada [27]. While the form (5-d) is an approximation to form (5-b) in the regime of weak output. The nonlinear gain is quantified by the coefficient ε of gain suppression.

Definitions of the parameters appearing in Eqs. (2.1) – (2.4) are as follows. τ_p is the photon lifetime, τ_{sp} is the spontaneous emission factor, τ_e is the spontaneous emission lifetime, I is the injection current, e is the electron charge, Γ is the confinement factor in the QW, $\Delta\nu(t)$ is the

frequency chirp, ν is the frequency of the oscillating mode, ν_o is the frequency of the cold mode in the laser resonator, and α is the linewidth enhancement factor.

Both the carrier transport time τ_{tr} and escape time τ_{esc} were found to be determined by the parameters of the SCH and well layers. The carrier transport across the SCH is characterized by the ambipolar diffusion time τ_{diff} and the capture time τ_{cap} in the QW [30], [31],

$$\tau_{tr} = \tau_{diff} + \tau_{cap} \tag{2.6}$$

The diffusion time is determined by the thickness L_{SCH} of the SCH layer and the ambipolar diffusion coefficient D_a as

$$\tau_{diff} = \frac{\tau_{SCH,hole} + \tau_{SCH,electron}}{2} = \frac{L_{SCH}^2}{2D_a} \tag{2.7}$$

The carrier capture time τ_{cap} is the duration of capturing carriers from the 3D states (SCH or the region above the well) to the 2D state (inside the well). Since the primary carrier type to be captured in the well is holes, the holes in the well attract more mobile electrons and increase the electron capture rate, simultaneously driving away other holes and reducing the hole capture rate. Therefore, the electron capture time is usually twice the hole capture time. Subpicosecond time-resolved measurements of the barrier luminescence decay in the GaAs-AlGaAs system, have determined the quantum carrier capture time to be 0.65ps for the holes and 1.2ps for the electrons and be independent of quantum-well width **[**32**].**

The carrier escape (or thermionic emission) τ_{esc} is the time that carriers escape from the 2D state (inside the well) to the 3D state (SCH layers). This time is an important parameter in determining the efficiency of QW lasers. If the carries obey Boltzmann statistics, the thermionic emission/escape time is determined by the thickness L_w of the QW as [33]

$$\tau_{esc} = \left(\frac{2\pi m^* L_W^2}{k_B T}\right)^{\frac{1}{2}} \exp\left(\frac{E_B}{k_B T}\right) \tag{2.8}$$

where m^* is the effective electron mass, k_B is the Boltzmann constant, T is the temperature in kelvin, and E_B is the effective barrier height.

The direct electrical current modulation of the QW laser is represented in Eq. (2.5) by combining both the biasing current I_b and the sinusoidal modulation component with amplitude I_m and frequency f_m,

$$I(t) = I_b + I_m \sin 2\pi f_m t \tag{2.9}$$

The above rate equations are linearized for the case of small-signal modulation that corresponds to $I_m << I_b$ [34]. Under this approximation, the linearization is achieved by writing the current $I(t)$, photon density $S(t)$, carrier densities $N(t)$ and $N_B(t)$ as

$$\begin{cases} I(t) = I_b + \Delta I_m(t) \\ S(t) = S_b + \Delta S(t) \\ N(t) = N_b + \Delta N(t) \\ N_B(t) = N_{Bb} + \Delta N_{Bm}(t) \end{cases} \tag{2.10}$$

and the gain *G(N,S)* is expanded by the Taylor expansion around the bias values N_b and S_b up to the second term as

$$G(N,S) = G_b(N_b,S_b) + \frac{\partial G}{\partial N}\Delta N + \frac{\partial G}{\partial S}\Delta S \tag{2.11}$$

By substituting Eqs. (2.9) and (2.10) into rate equations (2.1) – (2.4), and applying the Fourier transformation of the modulation amplitude:

$$\Delta X(t) = \int_{-\infty}^{\infty} X_m e^{j\Omega_m t} d\Omega_m \tag{2.12}$$

where X_m applies for the modulation amplitudes I_m, S_m, N_m, N_{Bm}, and $\Delta\nu_m$, and $\Omega_m = 2\pi f_m$ is the angular frequency, the following equations of the modulation components are derived:

$$\left(j\Omega_m - \Gamma S_b \frac{\partial G}{\partial S}\right) S_m = \left(\Gamma S_b \frac{\partial G}{\partial N}\right) N_m \tag{2.13}$$

$$\left[j\Omega_m + \left(\frac{1}{\tau_{esc}} + \frac{1}{\tau_e} + S_b \frac{\partial G}{\partial N}\right)\right] N_m = \frac{N_{bm}}{\tau_{tr}} - \left(S_b \frac{\partial G}{\partial S} + G_b\right) S_m \tag{2.14}$$

$$\left(j\Omega_m + \frac{1}{\tau_{tr}}\right) N_{Bm} = \frac{I_m}{e} + \frac{N_m}{\tau_{esc}} \tag{2.15}$$

$$\Delta\nu_m = \frac{\alpha}{4\pi}\Gamma \frac{\partial G}{\partial N} N_m \tag{2.16}$$

The steady-state components of *S*, *N*, and N_{Bb} and the chirp are determined from the following equations:

$$0 = \Gamma \mathrm{G}(N_b,S_b)S_b - \frac{S_b}{\tau_p} + \beta_{sp}\frac{N_b}{\tau_e} \tag{2.17}$$

$$0 = \frac{I_b}{e} - \frac{N_b}{\tau_e} - \mathrm{G}(N_b,S_b)S_b \tag{2.18}$$

$$N_{Bb} = \tau_{tr}\left(I_b + \frac{N_b}{\tau_{esc}}\right) \tag{2.19}$$

$$\Delta\nu_b = \frac{\alpha}{4\pi}\left(\Gamma G(N_b) - \frac{1}{\tau_p}\right) \tag{2.20}$$

It is worth noting that Eq. (2.19) indicates that the values of τ_{tr} should not increase the values of $\tau_{tr\,esc}$ to keep the injected carrier number in the barrier smaller than the carrier number in the QW.

By ignoring the spontaneous emission as it has a negligible contribution to the modulation response, the modulated components S_m, N_m , N_{Bm} and $\Delta\nu_m$ are derived as

$$S_m = \frac{\frac{\Gamma S_b \frac{\partial G}{\partial N}}{e\tau_{tr}} I_m}{-j\Omega_m\left(\Omega_m^2 - j\Omega_m \mathrm{A} - B\right) + \tau_{tr} C} \tag{2.21}$$

$$N_m = \frac{j\Omega_m - \Gamma S_b \frac{\partial G}{\partial S}}{\Gamma S_b \frac{\partial G}{\partial N}} S_m \tag{2.22}$$

$$N_{Bm} = \frac{\frac{I_m}{e} + \frac{N_m}{\tau_{esc}}}{j\Omega_m + \frac{1}{\tau_{tr}}} \tag{2.23}$$

$$\Delta\nu_m = \frac{\alpha}{4\pi S_b}\left(j\Omega - \Gamma S_b \frac{\partial G}{\partial s}\right) S_m \tag{2.24}$$

where the frequency components Ω_A, Ω_B^2, and Ω_C^3 are given by

$$\Omega_A = \frac{1}{\tau_e} + \frac{1}{\tau_{esc}} + \frac{1}{\tau_{tr}} + S_b\left(\frac{\partial G}{\partial N} - \Gamma\frac{\partial G}{\partial S}\right) \tag{2.25}$$

$$\Omega_B^2 = \frac{1}{\tau_e\tau_{tr}} + S_b\left(\frac{1}{\tau_p}\frac{\partial G}{\partial N} - \frac{\Gamma}{\tau_e}\frac{\partial G}{\partial S}\right) + S_b\left[\frac{1}{\tau_{tr}}\left(\frac{\partial G}{\partial N} - \Gamma\frac{\partial G}{\partial S}\right) - \Gamma\frac{\partial G}{\partial S}\frac{1}{\tau_{esc}}\right] \tag{2.26}$$

$$\Omega_C^3 = S_b\left(\frac{1}{\tau_p}\frac{\partial G}{\partial N} - \frac{\Gamma}{\tau_e}\frac{\partial G}{\partial S}\right) \tag{2.27}$$

The intensity modulation (IM) response at a specific bias current I_b and modulation frequency Ω_m is defined as the ratio of the modulated photon number $S_m(\Omega_m)$ to its value in the low-frequency regime, $S_m(\Omega_m \to 0)$,

$$IM(\Omega_m) = \frac{\Omega_C^3}{-j\Omega_m(\Omega_m^2 - \Omega_B^2) - \Omega_A\Omega_m^2 + \Omega_C^3} \tag{2.28}$$

Using this form, analytical expressions cannot be derived for the resonance frequency and damping rate in this form. The denominator is a third-order polynomial and can be solved numerically to determine the poles of the response. The bandwidth is determined as the 3dB frequency f_{3dB}, or the frequency at which the modulation response $|IM(\Omega)|$ drops to one-half of its value $|IM(\Omega_m \to 0)|$.

The chirp per modulated current ratio is then given in terms of $IM(\Omega_m)$ as

$$CCR = \frac{\Delta\nu_m}{I_m} = \frac{\alpha}{4\pi}\frac{\Gamma\frac{\partial G}{\partial N}}{e\tau_{tr}}\left(j\Omega_m - \Gamma S_b\frac{\partial G}{\partial s}\right)\frac{IM(\Omega_m)}{C} \tag{2.29}$$

The chirp is also characterized by the chirp-to-power ratio (CPR), which is a significant figure-of-merit for the chirp and is defined as the ratio of lasing frequency deviation to power deviation [18], and is given in this model as

$$CPR = \frac{\Delta\nu_m}{P_m} = \frac{\alpha}{4\pi P_b S_b}\left(j\Omega - \Gamma S_b\frac{\partial G}{\partial S}\right) \tag{2.30}$$

CPR is then controlled by the α-factor and varies linearly with the modulation frequency Ω_m. It is a complex quantity and its argument determines the phase shift of the frequency modulation from the intensit3y modulation.

3. NUMERICAL CALCULATION AND RESULTS:

The nonlinear form (6) of the optical gain in Eq. (2.5) is followed. The model is applied to 1.55μm-InGaAsP QW lasers [20]. The applied ranges of the transport and escape times correspond to varied values of thicknesses of both the SCH and QW. The values of τ_{tr} should not increase the values of $\tau_{tr\,esc}$ to keep the injected carrier number in the barrier N_b smaller than the carrier number N in the QW. In our previous paper [20], the transport processes in the SCH layer were limited only to the capture of carriers by the QW, and wide ranges of values were assumed for the escape and capture times which could make $N_b > N$.

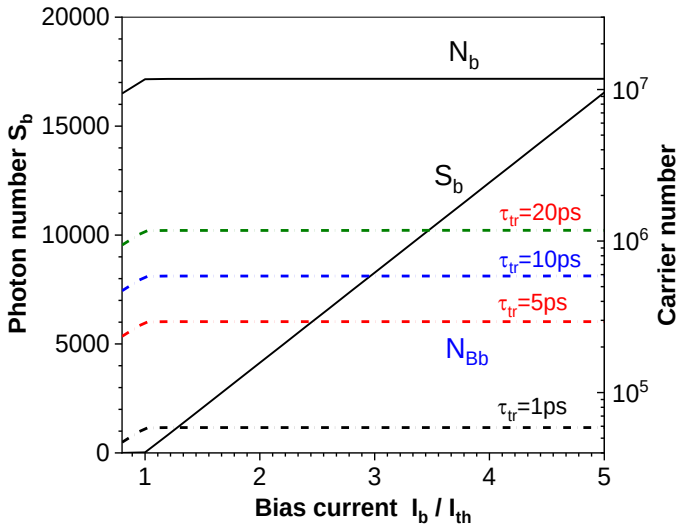

Figure 1. Plot of the steady state values of the photon density S_b, and the carrier densities N_b and N_{Bb} in the QW and SCH, respectively.

Figure 1 plots variations of the steady state values of the photon density S_b, and the carrier densities N_b and N_{Bb} in the QW and SCH, respectively. The escape time is set to be as long as τ_{esc} = 200ps to account for better modulation performance, while the transport time τ_{tr} ranges between 1 and 20ps. which could be controlled by controlling the thicknesses of the SCH layer and quantum well as given Eqs. (2.6) – (2.8) [10]. The figure shows a sudden change in the slope of the (S_b vs I_b), or the so-called "L-I" curve around the threshold level, which roots to the domination of the stimulated emission over the spontaneous emission. The threshold current of the QW laser under investigation is I_{th} = 63 mA. The variation of the carrier numbers N_b *and* N_{Bb} show that both of them are nearly constant in the above-threshold region and do not increase significantly with a further increase in I_b. The saturation of N corresponds to its value at the threshold, "threshold carrier number N_{th}", and the corresponding gain level is the threshold gain

$G_{th} = 1/\tau_p$. The figure shows also that neither S_b nor N_b changes with the variation of the transport time, while the carrier number N_{Bb} in the barrier region increases with the increase of τ_{tr}, as indicated in Eq. (2.19). This equation indicates also that N_{Bb} increases with decreasing the escape time τ_{esc}. In the following section, this increase of N_{Bb} will be shown as a main contributor to the limitation of the modulation performance.

In the following, the influence of the carrier transport phenomena on the modulation characteristics of the QW laser is investigated by varying the lifetimes τ_{esc} and τ_{tr}. Figures 2(a) and (b) plot the IM responses at different values of the transport time ranging between τ_{tr} = 1ps and 50ps under two extremes of the escape time; namely, the escape process is as slow as τ_{esc} = 200ps and as fast as τ_{esc} = 10ps, respectively. The bias current is set to be $I_b = 2I_{th}$. Both figures show the response is flat in the regime of low modulation frequencies, with increases of the modulation frequency in the regime of high frequencies attaining a maximum value at frequencies nearly equal to the resonance frequency of the laser. Then the response declines to much lower values beyond the response peak reaching a value of 3dB at the modulation bandwidth f_{3dB}. Also, the figures indicate that the IM response spectrum, including the values of the characteristic frequencies f_{3dB} and f_{peak}, changes with the variations of both τ_{tr} and τ_{esc}.

In figure 2(a) of τ_{esc} = 200ps, the IM response is lowered with the increase of τ_{tr}. While the peak frequency decreases a little from f_{peak} = 11.8 to 11.6GHz, the bandwidth decreases from f_{3dB} = 20.4 to 11.6GHz when the transport time increases from τ_{tr} = 1 to 50ps. On the other hand, figure 3(b) of τ_{esc} = 10ps indicates that the decrease of τ_{tr} is associated with not only shifting the IM response and the bandwidth f_{3dB} towards higher frequencies but also an increase in both the response peak and the peak frequency f_{peak}. As numeric examples, the characteristic frequencies are f_{peak} = 3GHz and f_{3dB} = 14.1GHz when τ_{tr} = 10ps, which increase to 16.5 and 19.5 GHz when τ_{tr} = 5 and 1ps, respectively.

Figures 3(a) and (b) plot the frequency spectra of the induced frequency chirp per modulated current ratio, CCR, as calculated via Eq. (2.29), which correspond to the transport and escape times in figure 2(a) and (b), respectively. Both figures show that the CCR spectrum increases with the increase of f_m, and exhibits a peak at the peak frequency f_{peak} of the IM response. The low-frequency regime is independent of the value of either τ_{tr} or τ_{esc}. Figure 3(a) indicates that the increase in τ_{tr} results in lowering the CCR spectrum, while the influence in figure 3(b) of shorter escape time τ_{esc} = 10ps is not only to reduce the spectrum but also to shift it to lower frequencies. That is, lower values of the frequency chirp are predicted at larger values of the transport time, while the escape time seems to have a minor impact. These effects are similar to

the variations of the IM response in figure 2. Finally, the figures indicate that the chirp ranges up to CCR = 26GHz/mA.

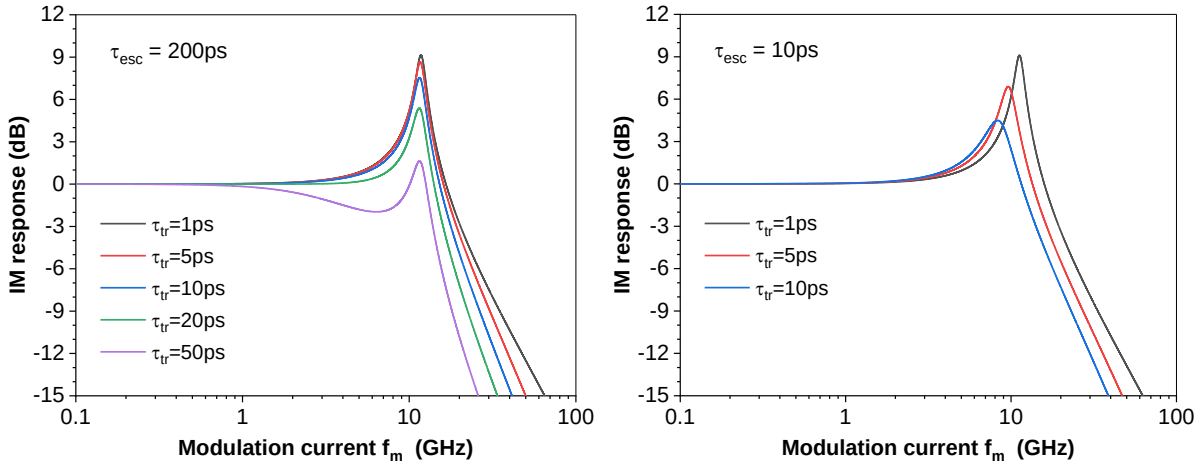

Figure 2. Plot of the IM response spectra at different values of the transport time τ_{tr} when the escape lifetime is (a) τ_{esc} = 100ps and (b) τ_{esc} = 10ps, with $I_b = 2I_{th}$.

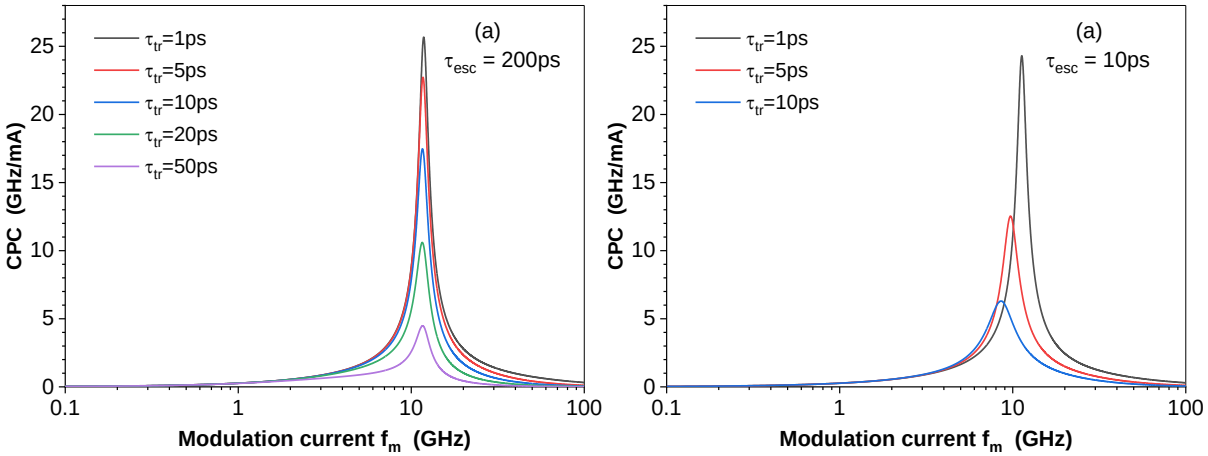

Figure 3. Plot of the frequency spectra of CCR at different values of the transport time τ_{tr} when the escape lifetime is (a) τ_{esc} = 200ps and (b) τ_{esc} = 10ps, with $I_b = 3I_{th}$.

The parameter of the chirp to modulated power ratio, CPR, evaluates the amount of variation of the lasing frequency that is associated or induced by the intensity modulation. Figure 4(a) plots the modulation spectrum of the magnitude of the complex CPR, as inferred from Eq. (2.30) over the relevant ranges of the lifetimes τ_{tr} and τ_{esc} using the same parameters of figures 2 and 3. As shown in the figure, the CPR increases linearly with the increase of the modulation frequency and is independent of the values of τ_{tr} and τ_{esc}, as indicated in Eq. (2.30). The phase of

the CPR quantity determines the phase change of the frequency chirp from the IM response. Figure 4(b) plots the corresponding CPR phase, showing that the frequency chirp is almost synchronized with the intensity modulation in the low-frequency regime. With the increase of the modulation frequency f_m, the figure shows that the phase changes to values around -1.5° (~0.48π), indicating a little lagging of the frequency variation behind the corresponding intensity modulation. This value is equal to $\tan^{-1}\frac{1}{\Gamma S_b \partial G/\partial S}$ as given in Eq. (2.30).

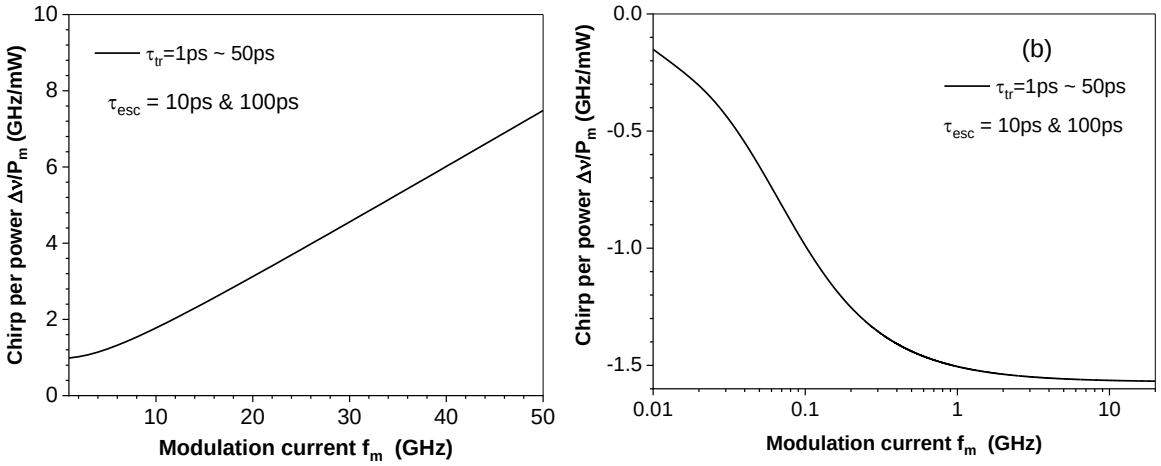

Figure 4. Plot of the frequency spectra of the frequency chirp CCR, (a) magnitude and (b) phase, over the entire ranges of the transport time τ_{tr} and escape time τ_{esc}.

Influences of the transport and escape processes on CCR and CPR are more illustrated in Figures 5(a) and (b), which plot the chirp values CCR_{peak} and CPR_{peak} calculated at the peak frequency of the QW over the entire ranges of τ_{esc} and τ_{tr} in Figure 3. The figures indicate that CCR_{peak} ranges between 0.3 and 4.7 GHz/mA while CPR_{peak} varies between 5 and 46 GHz/mW. Both CCR_{peak} and CPR_{peak} change with the lifetimes almost in a similar fashion to the bandwidth f_{3dB} in Figure 5. Both CCR_{peak} and CPR_{peak} decrease with the increase of τ_{tr} but increase with the increase of τ_{esc} up to τ_{tr}=20ps. τ_{tr}>20ps, CPR_{peak} is almost constant independent of the value of τ_{esc}. That is, the chirp values increase almost in a similar fashion to the bandwidth and decrease the carrier transport times τ_{esc} and τ_{tr} work to lower the frequency chirp associated with the intensity modulation for the laser. It is worth noting that the change of CPR_{peak} with both τ_{tr} and τ_{esc} despite the independence of CPR of τ_{tr} and τ_{esc} in Figure 4(a) is attributed to the corresponding change of the peak frequency f_{peak} as shown in Figure 3.

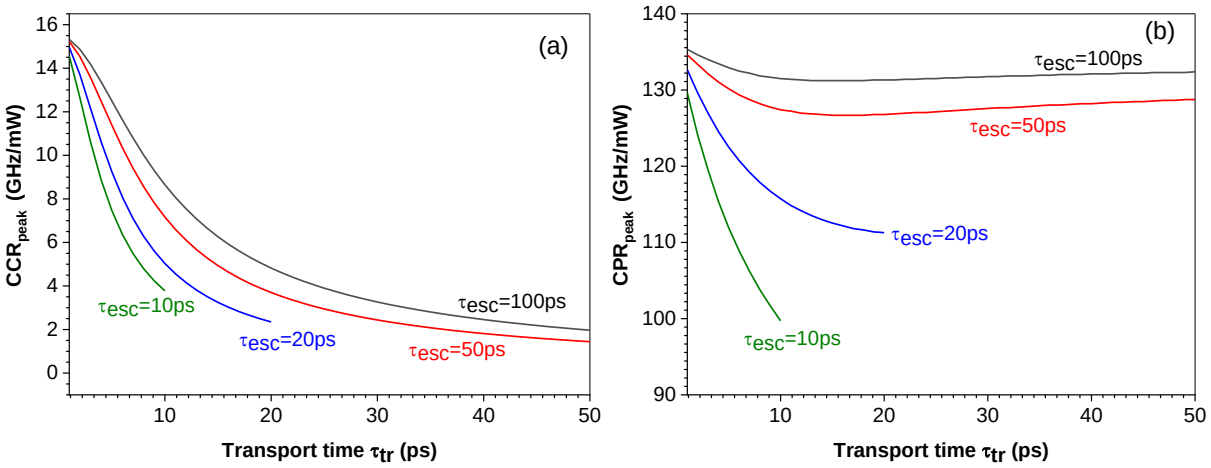

Figure 5. Plot of (a) frequency chirp per current CCR_{peak}, and (b) chirp per power ratio CPR_{peak} versus the transport time τ_{tr} at different values of the escape time τ_{esc}.

In Figure 6, the influence of the bias current I_b on the spectrum of CCR is illustrated. Figure 6 plots the frequency spectra of the chirp CCR at various bias currents of I_b =1.5 – 7.0 times the threshold level I_{th}. The values of the escape and transport times are fixed at τ_{esc} = 200ps and τ_{tr} = 2ps that correspond to high bandwidth f_{3dB}. The figures show the common effects of the bias current to shift the peak frequency of CCR to higher frequencies and to suppress the peak value of the spectrum, which is attributed to the increase of the damping rate of the laser. The calculated values of the chirp CCR_{peak} at the peak frequency range between 4 and 41 GHz/mA.

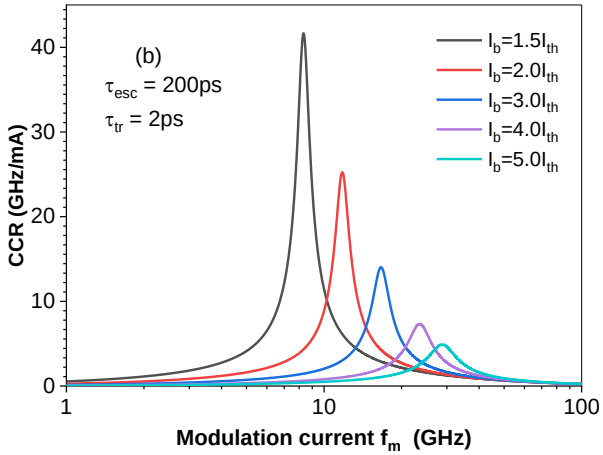

Figure 6. Plot of frequency chirp CCR at different values of the bias current I_b. The transport lifetime is τ_{tr} = 2ps and the escape lifetime is τ_{esc} = 200ps.

Figure 7(a) plots the magnitude of the complex CPR as a function of the modulation frequency f_m as a function of the bias current I_b. As shown in the figure, the slope of the linear relation of CPR versus f_m decreases with the increase of I_b, which is included in Eq. (2.30) as the slope is inversely proportional to S_b. Figure 7(b) plots the dependence of the phase of the CPR on current I_b. The figure shows that the phase change is negative; that is, the frequency chirp lags behind the intensity modulation. However, the magnitude of the phase change is less than 2° (0.63π), which indicates that the chirp is almost synchronized with the intensity modulation for the considered QW laser. The Figure shows that the increase of the current I_b shifts the frequency range over which the frequency chirp changes from almost synchronization to lagging behind the intensity modulation to higher frequency values. This shift is associated with a decrease in the value of the phase at the low-frequency regime. for example the phase shift is -0.16° when $I_b = 1.5I_{th}$ and decreases to -0.02° when $I_b = 7I_{th}$.

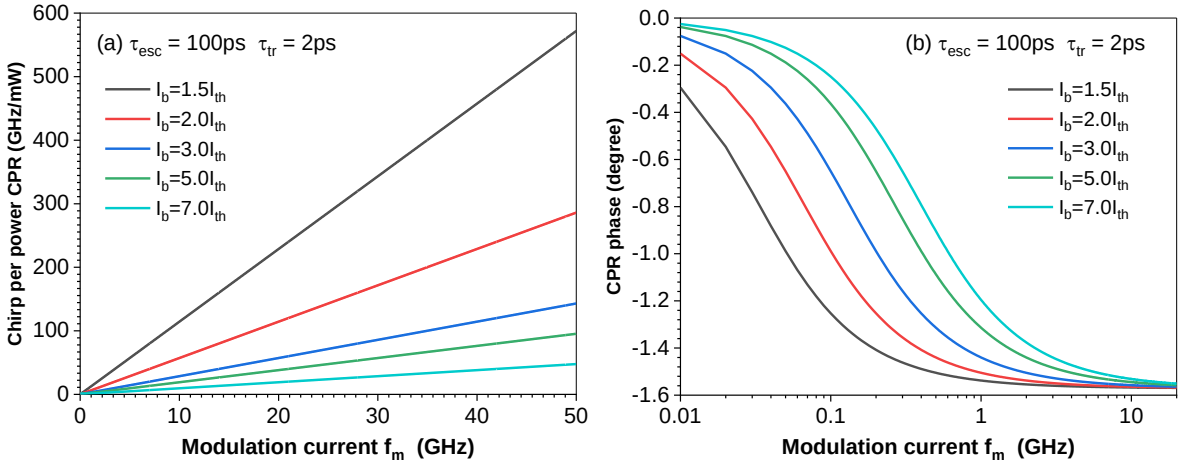

Figure 7. Influence of bias current I_b on (a) spectrum of CPR, and (b) phase of CPR, when τ_{tr} = 200ps with τ_{esc} = 2ps.

4. CONCLUSIONS

We developed a small-signal analysis model to linearize the coupled rate equations of modulated QW lasers incorporating the frequency chirp and the transport processes of charge carriers. Analytical forms were derived for both CCR and CPR as functions of the transport time in the SCH layer and escape time in the QW. The transport and diffusion processes of the charge carriers in the QW structure were shown to have significant impacts on the modulation bandwidth and the frequency chirp. The results showed that when the escape process is as slow as τ_{esc} = 200ps, the longer the transport time, the lower the bandwidth, and the higher the frequency chirp. When τ_{esc} = 10ps,

the decrease of τ_{tr} is associated with not only shifting the IM response and CCR spectrum and the bandwidth f_{3dB} towards higher frequencies but also an increase in the peak frequency. CPR increases linearly with the increase in the modulation frequency and is independent of the values of τ_{tr} and τ_{esc}. In the low-frequency regime, the frequency chirp is almost synchronized with the intensity modulation, whereas in the high-frequency regime, the frequency variation lags a little behind the intensity modulation. The values CCR at the peak frequency of the CCR spectrum, CCR_{peak}, ranges between 0.3 and 4.7 GHz/mA while CPR_{peak} varies between 5 and 46 GHz/mW. These chirp values decrease with the increase of τ_{tr} and decrease of τ_{tr} due to the corresponding change in the peak frequency.

Acknowledgment: This project was funded by the Deanship of Scientific Research (DSR) at King Abdulaziz University, Jeddah, under grant no. (GPIP: 1184-130-2024). The authors, therefore, acknowledge with thanks DSR for technical and financial support.

Conflicts of Interest: The author(s) declare that there are no conflicts of interest regarding the publication of this paper.

REFERENCES

[1] M.F. Ahmed, A.H. Bakry, F.T. Albelady, Digital Modulation Characteristics of High-Speed Semiconductor Laser for Use in Optical Communication Systems, Arab. J. Sci. Eng. 39 (2014), 5745–5752. https://doi.org/10.1007/s13369-014-1120-9.

[2] Z.-Y. Liu, T.-G. Zhao, Effect of Linewidth Enhancement Factor in Semiconductor Laser on Fiber Dispersion Transmission System, in: 2015 Fifth International Conference on Instrumentation and Measurement, Computer, Communication and Control (IMCCC), IEEE, Qinhuangdao, China, 2015: pp. 702–706. https://doi.org/10.1109/IMCCC.2015.153.

[3] R. Nagarajan, M. Ishikawa, T. Fukushima, R.S. Geels, J.E. Bowers, High Speed Quantum-Well Lasers and Carrier Transport Effects, IEEE J. Quantum Electron. 28 (1992), 1990–2008. https://doi.org/10.1109/3.159508.

[4] A.P. Wright, B. Garrett, G.H.B. Thompson, J.E.A. Whiteaway, Influence of Carrier Transport on Wavelength Chirp of InGaAs/InGaAsP MQW Lasers, Electron. Lett. 28 (1992), 1911–1913. https://doi.org/10.1049/el:19921223.

[5] M.O. Vassell, W.F. Sharfin, W.C. Rideout, J. Lee, Competing Effects of Well-Barrier Hole Burning and Nonlinear Gain on the Resonance Characteristics of Quantum-Well Lasers, IEEE J. Quantum Electron. 29 (1993), 1319–1329. https://doi.org/10.1109/3.236144.

[6] S.C. Kan, D. Vassilovski, T.C. Wu, K.Y. Lau, Quantum Capture and Escape in Quantum-Well Lasers-Implications on Direct Modulation Bandwidth Limitations, IEEE Photonics Technol. Lett. 4 (1992), 428–431. https://doi.org/10.1109/68.136475.

[7] S.C. Kan, D. Vassilovski, T.C. Wu, K.Y. Lau, Quantum Capture and Escape in Quantum-Well Lasers-Implications on Direct Modulation Bandwidth Limitations, IEEE Photonics Technol. Lett. 4 (1992), 428–431. https://doi.org/10.1109/68.136475.

[8] W. Rideout, W.F. Sharfin, E.S. Koteles, M.O. Vassell, B. Elman, Well-Barrier Hole Burning in Quantum Well Lasers, IEEE Photonics Technol. Lett. 3 (1991), 784–786. https://doi.org/10.1109/68.84492.

[9] R. Nagarajan, T. Fukushima, S.W. Corzine, J.E. Bowers, Effects of Carrier Transport on High-Speed Quantum Well Lasers, Appl. Phys. Lett. 59 (1991), 1835–1837. https://doi.org/10.1063/1.106213.

[10] R. Nagarajan, T. Fukushima, M. Ishikawa, J.E. Bowers, R.S. Geels, L.A. Coldren, Transport Limits in High-Speed Quantum-Well Lasers: Experiment and Theory, IEEE Photonics Technol. Lett. 4 (1992), 121–123. https://doi.org/10.1109/68.122335.

[11] R.F.S. Ribeiro, J.R.F. Da Rocha, A.V.T. Cartaxo, H.J.A. Da Silva, B. Franz, B. Wedding, FM Response of Quantum-Well Lasers Taking into Account Carrier Transport Effects, IEEE Photonics Technol. Lett. 7 (1995), 857–859. https://doi.org/10.1109/68.403980.

[12] E. Peral, W.K. Marshall, A. Yariv, Precise Measurement of Semiconductor Laser Chirp Using Effect of Propagation in Dispersive Fiber and Application to Simulation of Transmission through Fiber Gratings, J. Lightwave Technol. 16 (1998), 1874–1880. https://doi.org/10.1109/50.721075.

[13] E. Peral, A. Yariv, Measurement and Characterization of Laser Chirp of Multiquantum-Well Distributed-Feedback Lasers, IEEE Photonics Technol. Lett. 11 (1999), 307–309. https://doi.org/10.1109/68.748217.

[14] N. Otsuka, M. Kito, M. Ishino, Y. Matsui, 1.5-Mm Strained-Layer MQW-DFB Lasers with High Relaxation-Oscillation Frequency and Low-Chirp Characteristics, IEEE J. Quantum Electron. 32 (1996), 1230–1236. https://doi.org/10.1109/3.517023.

[15] P. Krehlik, Are Carrier Transport Effects Important for Chirp Modeling of Quantum-Well Lasers?, Adv. Electron. Telecommun. 1 (2010), 63-66.

[16] R.F.S. Ribeiro, J.R.F. Da Rocha, A.V.T. Cartaxo, H.J.A. Da Silva, B. Franz, B. Wedding, FM Response of Quantum-Well Lasers Taking into Account Carrier Transport Effects, IEEE Photonics Technol. Lett. 7 (1995), 857–859. https://doi.org/10.1109/68.403980.

[17] G.P. Agrawal, Fiber-Optic Communication Systems, Third ed., Wiley, New York, 2002.

[18] O. Doyle, P.B. Gallion, G. Debarge, Influence of Carrier Nonuniformity on the Phase Relationship between Frequency and Intensity Modulation in Semiconductor Lasers, IEEE J. Quantum Electron. 24 (1988), 516–522. https://doi.org/10.1109/3.156.

[19] J.J. He, Proposal for Q-Modulated Semiconductor Laser, IEEE Photonics Technol. Lett. 19 (2007), 285–287. https://doi.org/10.1109/LPT.2007.891242.

[20] M. Ahmed, M. Al-Alhumaidi, Influence of Carrier Transport on Modulation Characteristics of Quantum-Well Semiconductor Lasers, J. Comp. Electron. 22 (2023), 1140–1150. https://doi.org/10.1007/s10825-023-02060-6.

[21] A. Hangauer, G. Wysocki, Gain Compression and Linewidth Enhancement Factor in Mid-IR Quantum Cascade Lasers, IEEE J. Sel. Top. Quantum Electron. 21 (2015), 74–84. https://doi.org/10.1109/JSTQE.2015.2422073.

[22] A. Yousuf, H. Najeeb-ud-din, Effect of Gain Compression above and below Threshold on the Chirp Characteristics of 1.55 Mm Distributed Feedback Laser, Optical Rev. 23 (2016), 897–906. https://doi.org/10.1007/s10043-016-0268-9.

[23] A.G. Plyavenek, Combined Effect of Carrier Heating and Carrier Transport on the Intensity Modulation Response of Quantum Well Lasers, Optics Commun. 113 (1994), 259–271. https://doi.org/10.1016/0030-4018(94)90613-0.

[24] R. Nagarajan, T. Fukushima, J.E. Bowers, R.S. Geels, L.A. Coldren, Single Quantum Well Strained InGaAs/GaAs Lasers with Large Modulation Bandwidth and Low Damping, Electron. Lett. 27 (1991), 1058-1060.

[25] R.N. Hall, G.E. Fenner, J.D. Kingsley, T.J. Soltys, R.O. Carlson, Coherent Light Emission From GaAs Junctions, Phys. Rev. Lett. 9 (1962), 366–368. https://doi.org/10.1103/PhysRevLett.9.366.

[26] M. Yamada, Y. Suematsu, Analysis of Gain Suppression in Undoped Injection Lasers, J. Appl. Phys. 52 (1981), 2653–2664. https://doi.org/10.1063/1.329064.

[27] M. Ahmed, M. Yamada, An Infinite Order Perturbation Approach to Gain Calculation in Injection Semiconductor Lasers, J. Appl. Phys. 84 (1998), 3004–3015. https://doi.org/10.1063/1.368453.

[28] D.J. Channin, Effect of Gain Saturation on Injection Laser Switching, J. Appl. Phys. 50 (1979), 3858–3860. https://doi.org/10.1063/1.326510.

[29] G.P. Agrawal, Effect of Gain Nonlinearities on Period Doubling and Chaos in Directly Modulated Semiconductor Lasers, Appl. Phys. Lett. 49 (1986), 1013–1015. https://doi.org/10.1063/1.97456.

[30] G. Eisenstein, J.M. Wiesenfeld, M. Wegener, G. Sucha, D.S. Chemla, S. Weiss, G. Raybon, U. Koren, Ultrafast Gain Dynamics in 1.5 Mm Multiple Quantum Well Optical Amplifiers, Appl. Phys. Lett. 58 (1991), 158–160. https://doi.org/10.1063/1.105237.

[31] S. Weiss, J.M. Wiesenfeld, D.S. Chemla, G. Raybon, G. Sucha, et al. Carrier Capture Times in 1.5 Mm Multiple Quantum Well Optical Amplifiers, Appl. Phys. Lett. 60 (1992), 9–11. https://doi.org/10.1063/1.107426.

[32] S. Morin, B. Deveaud, F. Clerot, K. Fujiwara, K. Mitsunaga, Capture of Photoexcited Carriers in a Single Quantum Well with Different Confinement Structures, IEEE J. Quantum Electron. 27 (1991), 1669–1675. https://doi.org/10.1109/3.89991.

[33] H. Schneider, K.V. Klitzing, Thermionic Emission and Gaussian Transport of Holes in a GaAs/$A1_xGal_{1-x}$As Multiple-Quantum-Well Structure, Phys. Rev. B, 38 (1988), 6160-6165. https://doi.org/10.1103/physrevb.38.6160.

[34] M. Ahmed, A. El-Lafi, Analysis of Small-Signal Intensity Modulation of Semiconductor Lasers Taking Account of Gain Suppression, Pramana 71 (2008), 99–115. https://doi.org/10.1007/s12043-008-0144-7.